Bose-Einstein condensate as a diagnostic tool for an optical lattice formed by 1064-nm laser light

V. V. Tsyganok,[1] D. A. Pershin,[1,2] V. A. Khlebnikov,[1] D. A. Kumpilov,[1,3] I. A. Pyrkh,[1,4] A. E. Rudnev,[1,3] E. A. Fedotova,[1,3] D. V. Gaifudinov,[1,3] I. S. Cojocaru,[1,2] K. A. Khoruzhii,[1,3] P. A. Aksentsev,[1,4] A. K. Zykova,[1] and A. V. Akimov[1,2,5,*]

[1]*Russian Quantum Center, Bolshoy Boulevard 30, building 1, Skolkovo 143025, Russia*

[2]*PN Lebedev Institute RAS, Leninsky Prospekt 53, Moscow 119991, Russia*

[3]*Moscow Institute of Physics and Technology, Institutskii pereulok 9, Dolgoprudny, Moscow Region 141701, Russia*

[4]*Bauman Moscow State Technical University, 2nd Baumanskaya, 5, Moscow 105005, Russia*

[5]*National University of Science and Technology MISIS, Leninsky Prospekt 4, Moscow 119049, Russia*

(Received 17 March 2023; revised 24 May 2023; accepted 13 June 2023; published 11 July 2023)

Recently, thulium has been condensed to Bose-Einstein condensate. While the condensate of Thulium has a lot of applications in quantum simulations and other areas of physics, it can also serve as a unique diagnostic tool for many atomic experiments. In the present study, the Bose-Einstein condensate of Thulium was successfully loaded into an optical lattice and utilized to diagnose the lattice as well as detect unwanted reflections in the experiments with the 1064 nm optical lattice, which will further be used in a quantum gas microscope experiment.

DOI: 10.1103/PhysRevA.108.013310

I. INTRODUCTION

Ultracold atoms find more and more applications in sensing [1,2], time keeping [3–8], quantum computations [9–11], and quantum simulations [12–15]. The latter typically start with achieving a quantum degeneracy state. Among novel atoms that have just recently joined the family of atoms with achieved degeneracy, there is thulium [16], which possesses a lot of nonchaotic Fano-Feshbach resonances [17,18] at a low field and has a magnetic moment of 4 μ_B in the ground state. The presence of a large magnetic moment allows for long-range interaction, which is raising a large amount of interest in the scientific community [19–27] and has already allowed the observation of quantum chaos [20], the formation of ultracold polar molecules [28], and the observation of supersolids [29].

One of the effective approaches to quantum simulation is using a quantum gas microscope [15,30–35], which requires the formation of an optical lattice (OL). While the cooling of thulium could be done in both 532.07- and 1064-nm dipole traps with a little difference [36], the realization of a quantum gas microscope requires a larger separation between the nodes of an optical lattice, and therefore a 1064-nm light lattice is of interest. While working on the construction of such a device, there is a difficulty in the diagnostics of exact beam geometry. Although this question is solvable in principle, it is always useful to have an in-chamber probe, which can measure the actual configuration in a vacuum without opening the vacuum chamber. There have been a number of techniques suggested for addressing this problem, for example, the use of Ramsey imaging [37], the use of strong differential light shift [38], as well as the use of light induced shifts of atomic transitions [39], all utilizing specific properties of atoms in a vacuum chamber. On another side the Bose-Einstein condensate (BEC) is indeed a useful sensor for the configuration of laser beams, which does not depend much on the type of atoms condensed. The configuration of beams in the chamber could be imprinted on the matter wave of the condensate in position space via the Kapitza-Dirac (or Raman-Nath) effect [40–43]. The accumulated phase modulation could be transferred into momentum if the condensate is released. In the case of a periodic potential,

$$U(z) = U_0 \sin^2(k_L z), \tag{1}$$

where U_0 is the depth of the OL, $k_L = |\vec{k}_1 - \vec{k}_2|/2 = \pi/\lambda_L$ is one-half of the magnitude of the reciprocal lattice vector, $\vec{k}_1$ and $\vec{k}_2$ are wave vectors of OL beams, and $\lambda_L = \lambda/[2\sin(\alpha)]$ is a lattice period, $2\alpha = (\vec{k}_1; \vec{k}_2)$.

As the atoms are exposed to the pulse of periodic potential, they gain additional momentum, which could be detected during BEC expansion. The momentum gained by the atoms in the BEC is

$$\vec{p}_m = 2m\hbar\vec{k}_L, \quad m = 0, 1, 2..., \tag{2}$$

where $\hbar$ is a Planck constant and m is the diffraction order. The population of the mth diffracted order with $\vec{p}_m$ in the Raman-Nath regime [43] is a function of the exposure on the potential modulation T_p and OL depth U_0 as

$$P_m = J_m^2(U_0 T_p/2\hbar), \tag{3}$$

where J_m is the mth order Bessel function of the first kind. Thus, the distribution of momentum gained depends on both the pulse time and periodic potential depth. If the pulse time is known, the magnitude of the gained momentum carries information on the depth of the periodic potential. Moreover, the variation of the pulse time makes it possible to vary the sensitivity of the BEC to the potential depth, thus making it possible to focus on the specific range of depths.

The present study successfully utilized the Kapitza-Dirac effect on thulium atoms BEC to diagnose the OL and detect unwanted reflections in the experiments with the 1064-nm OL. The measurements were then verified by measurements of trap frequencies, calculated based on the results of the Kapitza-Dirac experiment.

*a.akimov@rqc.ru

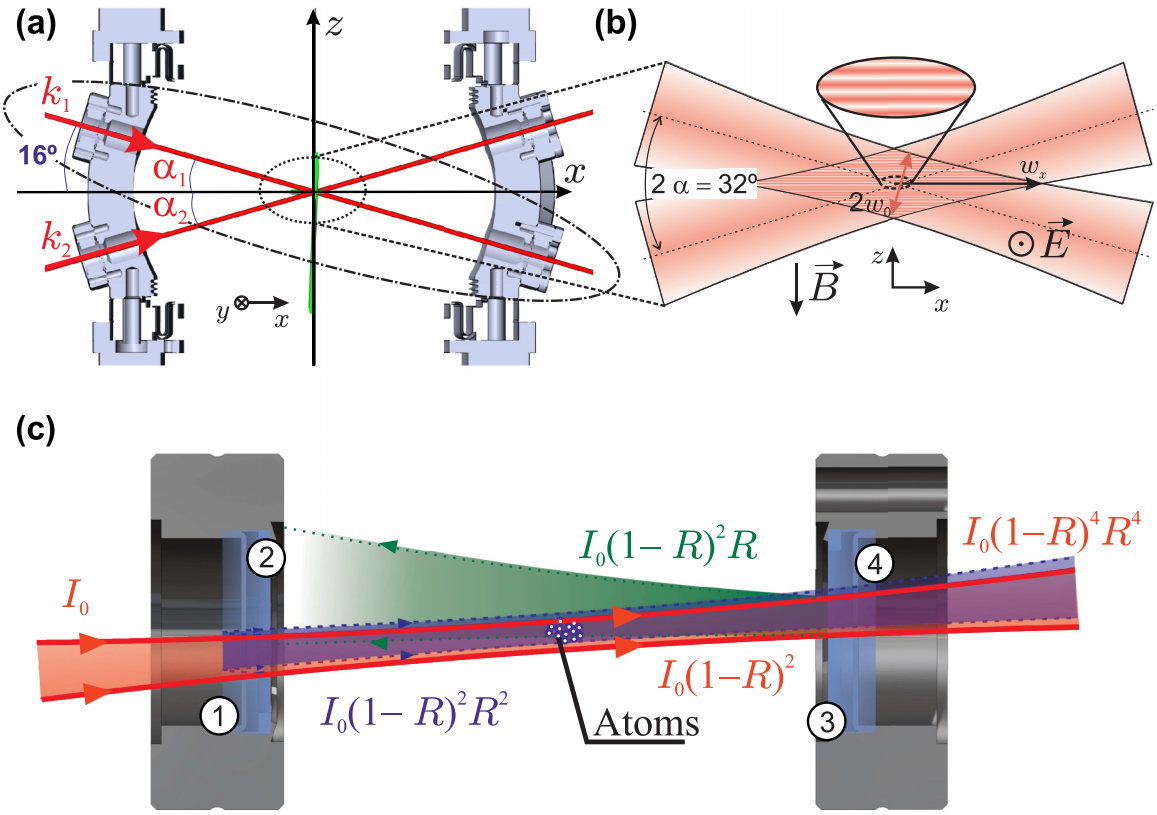

FIG. 1. (a) 1064-nm beams forming an optical lattice. (b) Details of the 1064-nm optical lattice. The polarization of the light is out of the plane of the figure. (c) Pair of viewport, marked with dash-dotted line at (a). The surfaces of the viewports are numbered ①, ②, ③, ④. Reflections of one beam of the optical lattice tilted at a slight angle to the surface 1. Red solid lines correspond to input and output beams with no reflection. Violet dashed lines correspond to the forward propagating reflection from the input viewport. Green dotted lines correspond to a reflected beam from the second viewport.

II. KAPITZA-DIRAC EXPERIMENT

The details of the experimental setup could be found elsewhere [16,17,44–48]. An atomic cloud was precooled in a magneto-optical trap, operating on $4f^{13}(^2F^o)6s^2 \rightarrow 4f^{12}(^3H_6)5d_{5/2}6s^2$ (530.7 nm) transition with precooling at $4f^{13}(^2F^0)6s^2 \rightarrow 4f^{12}(^3H_5)5d_{3/2}6s^2$ (410.6 nm) transition. Then atoms were loaded in a far-detuned magneto-optical trap [48] to form a cloud polarized to the lowest magnetic sublevel of the ground state $|F = 4; m_F = -4\rangle$. The cloud temperature after polarization was measured by the time-of-flight technique to be about 13 μK. Then atoms were loaded into a 532.07-nm optical dipole trap (ODT) with a waist size $w_z = 15.8\,\mu$m and $w_y = 25.7\,\mu$m as described in [47] and forced evaporatively cooled by decreasing the power of 532-laser beams [16]. Once BEC was achieved following the sequence described in [16], the atoms were used for further experiments.

The OL was formed by 1064-nm beams. The beams were crossed at $2\alpha \simeq 32^\circ$, leading to a vertical (along the z axis) lattice (see Fig. 1). The beams were focused into the region of the ODT with beam waists of $w_0 = 88 \pm 4\,\mu$m (at the e^{-2} level by power). The configuration was dictated by the geometry of the vacuum chamber (Kimball Physics MCF800-ExtOct-G2C8A16).

BEC served two purposes: First, it was used to check the presence of a 1064-nm OL, and second, to diagnose unwanted reflections, which unfortunately were present due to the absence of an antireflection coating. Viewports that were used in the OL setup had an antireflection coating for 532.07 nm but not for 1064 nm. The reflection coefficient R of the window was verified using a spare window and was found to be $R = 15.5 \pm 1.7\%$ using the reflection of the same laser beam used for the OL. This reflection coefficient is significant and thus unwanted reflections may significantly modify the parameters of an OL.

To form the OL, the beams were adjusted in two steps: first, both beams were aligned to be perpendicular to the vacuum chamber viewports [see Fig. 1(a)] by matching the reflection from both surfaces of the port and the beam. Then the beams were intersected inside the vacuum chamber and moved to the location of BEC (formed at 532.07-nm ODT) by observing the reloading of the atomic cloud into a 1064-nm OL. Once the beams were aligned perpendicularly to the viewport, the angle of incidence for the beams could not be changed significantly. The setup has fused silica viewports with a window diameter of 16 mm and thickness of 1.8 mm. The distance between windows is 221.3 mm. The waist of the beam on the window at the level e^{-5} is 0.7 mm. Thus, the angles of incidence for the beams α_1, α_2 cannot be more than

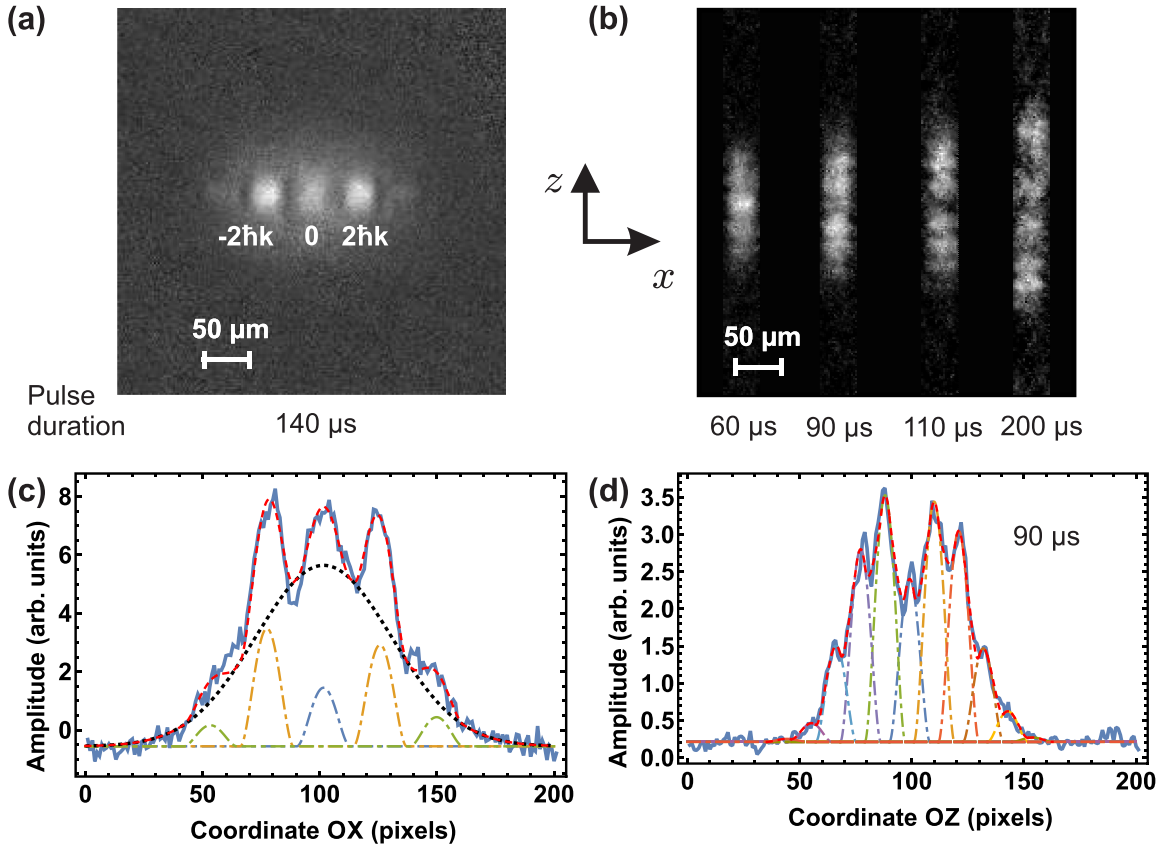

FIG. 2. (a) 15-ms expansion of BEC after 140-μs pulse of a single OL beam with a power of 0.8 W. (b) 15-ms expansion of BEC after 60-, 90-, 110-, and 200-μs pulse of the OL. (c) Horizontal cross section of image (a). (d) Vertical cross section of image (b), 90 μs. For both (c) and (d) the red dashed line is a fit with Eq. (4) with $i = 2$ for (c) and $i = 5$ for (d). The dotted black line is a fit of the thermal cloud. Dot-dashed lines are the fit of diffraction peaks.

$16^\circ \pm 3.7^\circ$. The viewports themselves are located 16° with respect to the horizontal xy plane.

Due to the alignment procedure, there is a good chance of strong overlap of the OL beam and its forward reflection from the viewport for each of the beams [the beam was limited by violet arrows, Fig. 1(c)], forming the unwanted extra OL. Besides, there is a possibility of the reflection from the second viewport [green beam, Fig. 1(c)].

The "green" reflection will expand between surfaces 3 and 2 considerably but in the position of the OL region, the expected beam size is still about 830 μm and is thus not negligible.

Exact geometrical measurements, though possible, are quite challenging for the vacuum volume which is part of the optical setup. However, the beam geometry may be analyzed using the interference of BEC using the Kapitza-Dirac effect. This analysis was performed first for a single lattice beam [Fig. 2(a)] and then for both OL beams along $\vec{k}_1$ and $\vec{k}_2$ [Fig. 2(b)].

To check the unwanted lattices formed by self-reflections of individual beams, atoms were first cooled to the BEC state at the 532.07-nm ODT. Then, while the ODT was still on, one OL [$\vec{k}_1$ in Fig. 1(a)] beam of interest was turned on for 140 μs. The power of one ODT beam was 1.1 W before the vacuum chamber. Once the OL beam was turned off, the 532.07-nm ODT was turned off as well, and the cloud expanded freely for 15 ms. After expansion the BEC cloud experienced diffraction due to the phase, accumulated during interaction with the lattice and thus formed the picture presented in Fig. 2(a). The presence of this picture indeed confirms that the reflection from viewport windows do form unwanted lattice. The m-spot picture corresponds to the momentum, gained by BEC while interacting with the OL beam, namely $|2m\hbar\vec{k}_l\rangle$, $m = 0, 1, 2...$, where $\vec{k}_l$ is the wave vector of the periodic lattice, present in the beam due to the self-reflection of the beam. Figure 2(c) shows the fit of the one-dimensional atomic distribution with ($i = 2$):

$$N(x) = bg + \frac{N_t}{\sigma_x\sqrt{\pi}} \exp\left[-\frac{(x-x_0)^2}{\sigma_x^2}\right] + \begin{cases} \sum_{m=-i}^{i} \frac{15N_m}{16R}\left(1 - \frac{(x-x_0+m\Delta)^2}{R^2}\right)^2, & x - x_0 + m\Delta \leqslant R \\ 0, & x - x_0 + m\Delta \geqslant R \end{cases}, \tag{4}$$

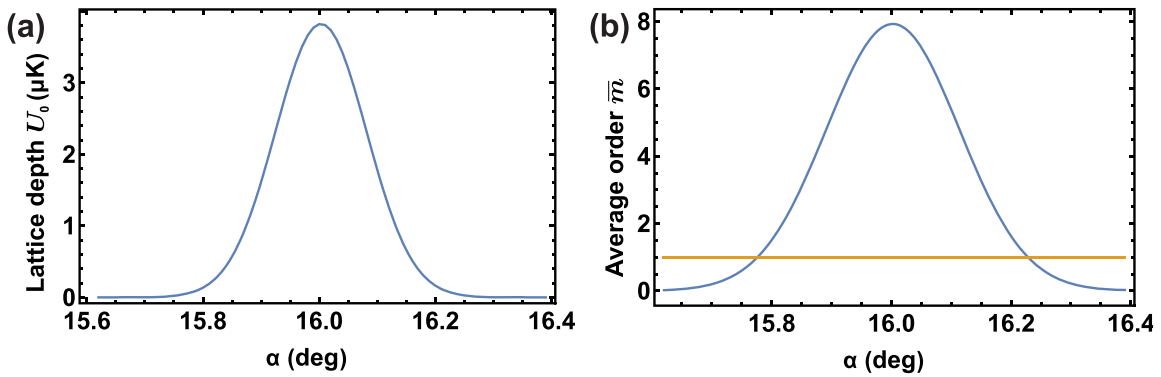

FIG. 3. (a) Calculated dependence of the unwanted lattice depth versus angle based on geometry of the setup. (b) The highest order of BEC diffraction picture calculated using (a) and Eq. (6).

where bg is a background, N_t is the number of atoms of the thermal part, σ_x is a cloud size of the thermal cloud, x_0 is the position of the center of mass, N_m is the number of atoms of the mth diffraction order, R is a BEC radius, and Δ is a distance between the nearest diffraction orders. The value of Δ could also be calculated as

$$\Delta = \frac{2\hbar k_L}{M_{\mathrm{Th}}} t, \tag{5}$$

where M_{Th} is the thulium mass and t is the time of flight. According to the fit, $\Delta_{\mathrm{exp}} = 47 \pm 2\,\mu\mathrm{m}$ and is in good agreement with theory [Eq. (5)] where $\lambda_L = 532$ nm and $\Delta = 46\,\mu\mathrm{m}$.

In order to have interference of two beams those should overlap. In our geometry if both forward and back reflected beams overlap exactly it would correspond to the angle $\alpha = 16^\circ$. At this angle we expect windows to be exactly perpendicular to the beam and thus the reflection should overlap with the incoming beam forming the strongest possible horizontal lattice. As the angle changes the overlap between forward propagating beam and a back reflecting beam decrease, leading to the reduction of the lattice contrast. The use of BEC allows to estimate this angle through the analysis of the interference fringes. Since interference fringes are sensitive to the depth of the optical lattice (3), one could ask what is the minimal intensity at which the diffraction will happen at all. The highest order of BEC diffraction picture $\bar{m}$ could be expressed [43] as

$$\bar{m} = \sqrt{\beta/\gamma}, \quad \beta = \frac{U_0 T_p}{\hbar}, \quad \gamma = 2\frac{\hbar k_L^2}{M_{Th}} T_p. \tag{6}$$

From this formula one could see, that if the depth of the lattice is less, that value required for having at least one diffraction order, the interference pattern would not happen. Thus, the critical depth of the trap is

$$U_0 = \frac{2(\hbar k_L)^2}{M_{Th}}, \tag{7}$$

which simply means there should be at least one two-photon recoil event. The trap depth may be expressed for our geometry as a function of angle α [see the Modeling section and Eqs. (8)–(13) and Fig. 3(a)]. For beam $\vec{k}_1$ Eq. (7) may be solved with respect to the angle α and has two solutions, 15.8° and 16.2° [see Fig. 3(b)]. Thus, presence of the unwanted lattice, formed by reflections, indicated in Fig. 1(c) sets condition $15.8^\circ < \alpha_1 < 16.2^\circ$. Forward reflection also modifies the beam intensity.

The single $\vec{k}_2$ beam [Fig. 1(a)] does not make any horizontal diffraction pictures of BEC at any beam power. Therefore, one can exclude that the geometry of this beam makes an intersection with self-reflection from surfaces 3 and 4 [Fig. 1(b)] and the angles for that beam could be $13.1^\circ < \alpha < 15.8^\circ$ and $16.2^\circ < \alpha < 18.9^\circ$.

Two beams with wavelength 1064 nm should form an OL with wave vector k_L along the z axis in the laboratory frame [see Fig. 1(b)]. Indeed, if the Kapitza-Dirac type experiment is repeated with both beams forming the OL, one could see BEC diffraction peaks in a vertical direction [Fig. 2(b)]. In this case, the OL was turned on only for 60, 90, 110, and 200 μs since the interference pattern was expected to have a large depth (the power at each OL beam was 0.54 W before the vacuum chamber), and therefore less exposure was needed. Reduced exposure also significantly reduced the visibility of the horizontal peaks. Figure 2(d) shows a one-dimensional fit with Eq. (4) ($i = 5$) of the data corresponding to the 90-μs exposition of the OL. The value of $\Delta_e = 17 \pm 2\,\mu\mathrm{m}$ obtained from the fit is also in good agreement with theory $\Delta = 17\,\mu\mathrm{m}$ for $\lambda_L = 1064\ \mathrm{nm}/2\sin[16^\circ] = 1930$ nm [see Eq. (5)].

III. MODELING

The result of the measurements showed that only one of the beams forming OL had a reflection from the second viewport (surface 3), marked as green in Fig. 1(c), that overlaps with the BEC. This is perfectly within what is possible in the setup, but hard to check directly. To model the potential, only two reflections for one beam $\vec{k}_1$ [see Fig. 1(c)] and one reflection for beam $\vec{k}_2$ were used, as the next order of reflection is too small to significantly affect the BEC during the exposure time used. The full value of the electric field $\vec{E}_{\mathrm{SUM}}$ in the cross region in this model would be

$$\vec{E}_{\mathrm{SUM}} = \vec{E}_{10} + \vec{E}_{11} + \vec{E}_{13} + \vec{E}_{20} + \vec{E}_{21}, \tag{8}$$

where the first index i in $\vec{E}_{ij}$ is the number of the OL beams, and the second index j is the number of reflecting surfaces

as those marked in Fig. 1(c); 0 stands for no reflection. The relative amplitudes of the transmitted and reflected beams may be calculated as indicated below [as the reference frame, the one indicated in Fig. 1(b) was used]:

$$\vec{E}_{10} \propto \vec{E}_{20} \propto \left\{0, \sqrt{\frac{2I_0(1-R)^2}{\varepsilon_0 c}}, 0\right\} \frac{1}{\sqrt{1+\left(\frac{\lambda x_{1,2}}{\pi\omega_0^2}\right)^2}} \exp\left[-\frac{(z_{1,2})^2+y^2}{\omega_0^2\left(1+\left(\frac{\lambda(x_{1,2})}{\pi\omega_0^2}\right)^2\right)}\right] \exp[i(\vec{k}_{1,2},\vec{r})], \tag{9}$$

$$\vec{E}_{11} \propto \vec{E}_{21} \propto \left\{0, \sqrt{\frac{2I_0(1-R)^2R^2}{\varepsilon_0 c}}, 0\right\} \frac{1}{\sqrt{1+\left(\frac{\lambda(x_{1,2}+\delta_1)}{\pi\omega_0^2}\right)^2}} \exp\left[-\frac{z_{1,2}^2+y^2}{\omega_0^2\left(1+\left(\frac{\lambda(x_{1,2}+\delta_1)}{\pi\omega_0^2}\right)^2\right)}\right] \exp\left[i\left(\vec{k}_{1,2},\vec{r}+\frac{2\pi}{\lambda}\delta_1\right)\right], \tag{10}$$

$$\vec{E}_{13} \propto \left\{0, \sqrt{\frac{2I_0(1-R)^2R}{\varepsilon_0 c}}, 0\right\} \frac{1}{\sqrt{1+\left(\frac{\lambda(x_{13}+D/2)}{\pi\omega_0^2}\right)^2}} \exp\left[-\frac{z_{13}^2+y^2}{\omega_0^2\left(1+\left(\frac{\lambda(x_{13}+D/2)}{\pi\omega_0^2}\right)^2\right)}\right] \exp\left[i\left(\vec{k}_{13},\vec{r}+\frac{2\pi}{\lambda}\delta_2\right)\right], \tag{11}$$

where the following notation been used:

$$\begin{aligned}
x_1 &= x\cos[\alpha] + z\sin[\alpha]\\
x_2 &= x\cos[\alpha] - z\sin[\alpha]\\
z_1 &= -x\sin[\alpha] + z\cos[\alpha],\\
z_2 &= x\sin[\alpha] + z\cos[\alpha],\\
x_{13} &= \cos[32^\circ-\alpha]\left(-x+\frac{D}{2}\cos[\alpha]\right) - \sin[32^\circ-\alpha]\left(z-\frac{D}{2}\sin[\alpha]\right),\\
z_{13} &= \left(-x+\frac{D}{2}\cos[\alpha]\right)\sin[32^\circ-\alpha] + \cos[32^\circ-\alpha]\left(z-\frac{D}{2}\sin[\alpha]\right),\\
\delta_1 &= 2nd\sqrt{1-(\sin[\alpha-16^\circ]/n)^2},
\end{aligned} \tag{12}$$

and $\vec{k}_{1,2}, \vec{k}_{13}$ are wave vectors of beams and reflected beams, is the optical path difference arising in the window with the index of refraction n and thickness d, and $\delta_2 = D$ is the optical path difference arising in the vacuum chamber with a diameter D.

The depth of the OL is

$$\begin{aligned}
U_{OL}(x,y,z,\alpha) &= -\frac{2\pi a_B^3}{c}\mathrm{Re}(\alpha_{\mathrm{tot}})I(x,y,z,\alpha),\\
I(x,y,z,\alpha) &= \frac{\varepsilon_0 c}{2}|\vec{E}_{\mathrm{SUM}}(x,y,z,\alpha)|^2,
\end{aligned} \tag{13}$$

where ε_0 is the vacuum permittivity, a_B–Bohr radius. In the simulations, the input fields of both beams forming the OL were assumed to be the same. The simulated beam OL profile is indicated in Fig. 4(a). Here, the value for polarizability was taken from [36], and the field magnitude was found from the experimentally measured beam powers and experimentally found beam waist, $\omega_0 = 88 \pm 4\,\mu\mathrm{m}$.

To test the modeled OL structure, one could perform measurements of the trap frequency (ν_x, ν_y, ν_z) (see below). In a parabolic approximation, to find trap frequencies, one needs to calculate the second derivative of the potential:

$$\nu_i = \frac{1}{2\pi}\sqrt{\frac{1}{m_{th}}\frac{\partial^2 U_{\mathrm{OL}}}{\partial i^2}}, \qquad i \in \{x,y,z\}. \tag{14}$$

IV. TRAP FREQUENCIES IN THE OPTICAL LATTICE

To measure the trap frequencies of the OL, formed by a laser beam with a wavelength of 1064 nm, the following experiment was performed: First, atoms were loaded into a 532.07-nm ODT without waiting for the end of evaporation cooling. Then the power of 1064-nm OL laser beams was increased up to 4.0, 5.3, or 5.9 W per beam in a vacuum chamber (depending on the experiment) to reload atoms into the OL [see Fig. 4(b)]. The time duration of this stage was 2.2 s. Typically, about 1.0×10^6 atoms with a temperature of 10 μK were loaded into the OL. The magnetic field during the entire stage remained constant and was equal to −3.91G along the Oz axis [Figs. 1(a) and 1(b)]. An atomic cloud was then held in the OL for about 1 s, and then the measurement step was performed.

To measure the frequency of the OL, the parametric heating [49,50] of an atomic cloud was used. Such heating was implemented by the modulation of both 1064-nm laser beams [see inset in Fig. 4(b)]. The OL modulation was turned on for about 1.6 s using an acousto-optic modulator with a small modulation index of 5% by power of beams. Once modulation was completed, the remaining number of atoms was detected. The experiment was repeated for various modulation frequencies and power of OL beams demonstrated in Fig. 4(c).

The trap frequencies ν_i were determined from the minimum of the obtained curve ν_{OL} as

$$\nu_i = \frac{\nu_{\mathrm{OL}}}{2}, \tag{15}$$

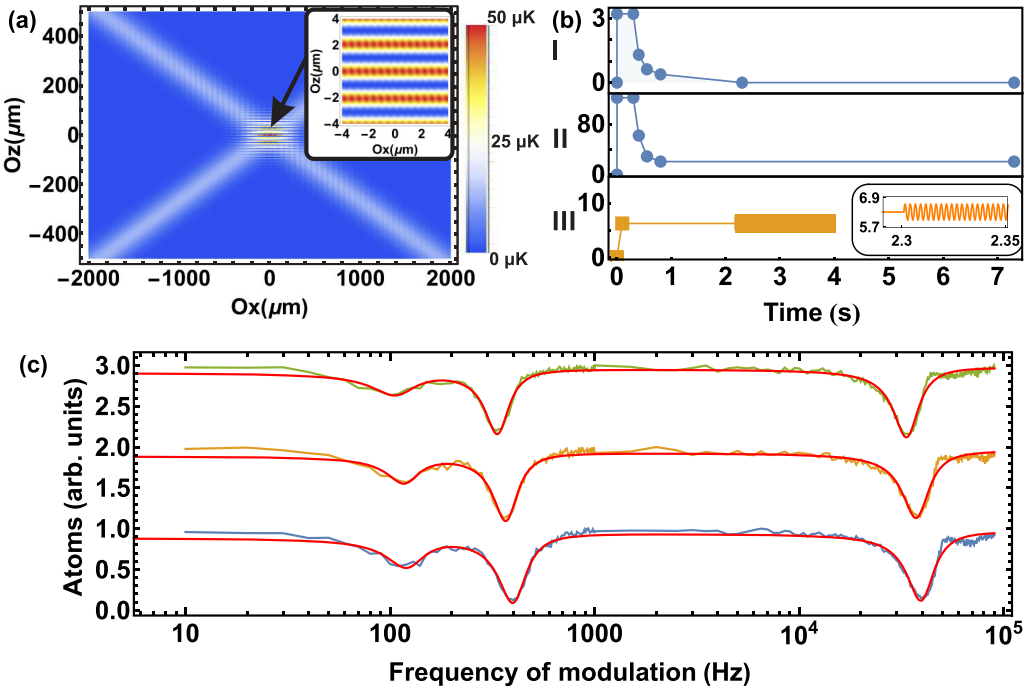

FIG. 4. (a) Reconstructed potential at the Oxz plane. The powers of light beams are assumed to be the same. The angles taken are $\alpha_1 = 16^\circ$, $\alpha_2 = 15.8^\circ$. (b) Pulse scheme of the parametric heating experiment. I: power of the horizontal 532-nm ODT beam in W; II: ODT beam scanning in μm; III: power per one OL beam. (c) Atom loss during 1.6 s of power modulation of 1064-nm laser beams. Green, orange, and blue dots correspond to experimental data with power at one beam of 4.0, 5.3, and 5.9 W. Lines fit experimental data with three Lorentzian functions.

where i represents x, y, z. The measured frequencies were found to be [see Fig. 4(c)] as in Table I.

Thulium has high angular momentum J in the ground state leading to relatively large role of tensor polarizability in total polarizability of an atom and thus in trap frequency. The tensor part of the polarizability depends on the angle between the quantization axis set by the direction of the magetic field and the direction of linear polarization of the beams. As ν_Z has the most sensitivity to the tensor part of the polarizability, the shift of parametric resonance is measured to check tensor polarizability. The measurements were performed for two different orientations of the magnetic field. The first one was done for the magnetic field -3.91G oriented along the Oz axis, and the second one for the magnetic field 3.91 G oriented along the Oy axis [Fig. 5(a)]. Due to asymmetry in resonance shape the frequencies were found by parabolic fit near local minima and were found to be 40.3 ± 0.1 kHz and 39.7 ± 0.2 kHz, correspondingly. Thus, the polarizability ratio $\alpha_{\mathrm{VERT}\,B}/\alpha_{\mathrm{HOR}\,B} = (\nu_{Z\,\mathrm{VERT}\,B}/\nu_{Z\,\mathrm{HOR}\,B})^2$ was found to be about 0.97 ± 0.03 from the experiment, which is close to previous experimental results of 0.97 ± 0.3 [7,36].

TABLE I. OL frequencies from experimental data.

Power	4.0 W	5.3 W	5.9 W
ν_x	52 ± 3 Hz	58 ± 3 Hz	61 ± 3 Hz
ν_y	167 ± 2 Hz	184 ± 2 Hz	199 ± 2 Hz
ν_z	16.7 ± 0.1 kHz	18.6 ± 0.1 kHz	19.6 ± 0.2 kHz

Figure 5(b) shows the experimentally found trap frequencies along with the simulated frequencies as a function of an angle α_2 [see Fig. 1(a)] between the k_2 beam of the OL and horizontal plane. The frequency ν_z was calculated for the power of 4.0 W per beam using scalar and tensor polarizabilities from [36] and the model (8)–(14). Oscillations of the calculated trap frequency are caused by the phase between the fields $\vec{E}_{10}$, $\vec{E}_{20}$ and $\vec{E}_{11}$, $\vec{E}_{21}$, respectively, as it depends on the angle of incidence on the window $\alpha_2 - 16^\circ$. The oscillatory behavior of the model leads to three possible solutions for the angle α_2, only one of which is excluded by the BEC experiment.

The polarizability of thulium was measured with finite precision [36]. Mostly, the systematic uncertainty of the experiments leads to the uncertainty of the calculated value of polarizability. Nevertheless, since polarizability was measured in the same setup and was measured via measurements of trap frequencies, thus, in reality, the comparison of trap frequencies with trap frequencies at the same setups and therefore the systematic uncertainty of the polarizability measurements may be excluded from consideration. To estimate the tolerance interval of angle α, calculations of the polarizabilities were done for mean value of polarizability, and also for the values, bounding the statistical uncertainty range of palatability. Angles, found from later values, thus were used as a border of tolerance interval for angles found. The same procedure was repeated for all sets of powers from Fig. 4(c) and for trap frequencies in all three directions. The intersection of allowed ranges of angles exists for all these measurements

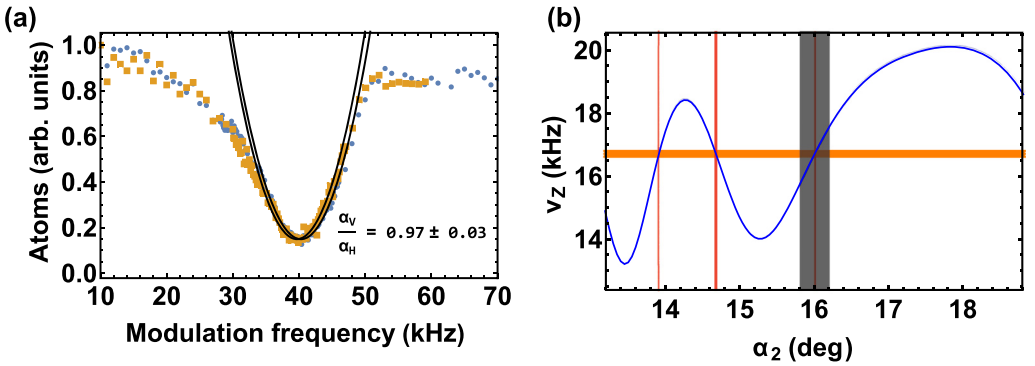

FIG. 5. (a) Dependence of atom loss versus the frequency of modulation in two different cases of the magnetic field. Blue dots correspond to the Oz direction of the magnetic field while orange dots correspond to the horizontal (Oy) direction of the magnetic field. Black lines represent the fit of the data with parabola near local minima. (b) Frequency ν_z from model Eq. (14) versus the angle of the second beam α_2 for the power 4.0 W per beam. The first beam has an angle of 16°. The blue solid line is the result of the calculation for trap frequency. The orange horizontal line shows the frequency of 16.7 ± 0.1 kHz measured experimentally. The grey rectangle represents the area, which is excluded from the model due to the experiment with BEC diffraction. Red vertical lines show regions in which frequency from the model coincides with the experimental results within the error bar.

which we take as the final value for α_2: $\alpha_2 = 13.83° \pm 0.15°$, $\alpha_2 = 14.75° \pm 0.13°$.

If systematic uncertainty must be taken into account, it will significantly reduce the precision with which the angle could be found, but it could be corrected by the measurement of trap frequency with a known beam at the same setup.

V. CONCLUSIONS

A thulium BEC was successfully loaded into an optical lattice, opening a possibility to perform quantum simulation on a lattice with it. The condensate was used to diagnose the parameters of the lattice using the Kapitza-Dirac effect. It was determined that one of the lattice beams had self-reflection, interfering with the main lattice. The period of this lattice as well as the period of the main lattice were extracted from BEC diffraction images and were consistent with the results of a numerical model. The validity of the lattice picture reconstruction was checked via polarizability measurements and was found to be consistent with the previously measured value. Moreover, the angle of incidence of one of the beams was restricted to two discrete values using the combination of BEC diffraction data and trap frequency measurements.

ACKNOWLEDGMENT

This work was supported by Rosatom in the framework of the Roadmap for Quantum computing (Contract No. 868-1.3-15/15-2021 dated October 5, 2021).

[1] W. F. McGrew, X. Zhang, R. J. Fasano, S. A. Schäffer, K. Beloy, D. Nicolodi, R. C. Brown, N. Hinkley, G. Milani, M. Schioppo, T. H. Yoon, and A. D. Ludlow, Nature (London) **564**, 87 (2018).

[2] D. Becker, M. D. Lachmann, S. T. Seidel, H. Ahlers, A. N. Dinkelaker, J. Grosse, O. Hellmig, H. Müntinga, V. Schkolnik, T. Wendrich *et al.*, Nature (London) **562**, 391 (2018).

[3] T. Bothwell, D. Kedar, E. Oelker, J. M. Robinson, S. L. Bromley, W. L. Tew, J. Ye, and C. J. Kennedy, Metrologia **56**, 065004 (2019).

[4] N. Nemitz, T. Ohkubo, M. Takamoto, I. Ushijima, M. Das, N. Ohmae, and H. Katori, Nat. Photon. **10**, 258 (2016).

[5] R. Hobson, W. Bowden, A. Vianello, A. Silva, C. F. A. Baynham, H. S. Margolis, P. E. G. Baird, P. Gill, and I. R. Hill, Metrologia **57**, 065026 (2020).

[6] A. A. Golovizin, D. O. Tregubov, E. S. Fedorova, D. A. Mishin, D. I. Provorchenko, K. Y. Khabarova, V. N. Sorokin, and N. N. Kolachevsky, Nat. Commun. **12**, 5171 (2021).

[7] A. Golovizin, E. Fedorova, D. Tregubov, D. Sukachev, K. Khabarova, V. Sorokin, and N. Kolachevsky, Nat. Commun. **10**, 1724 (2019).

[8] A. Golovizin, D. Tregubov, D. Mishin, D. Provorchenko, N. Kolachevsky, and N. Kolachevsky, Opt. Express **29**, 36734 (2021).

[9] S. R. Cohen and J. D. Thompson, PRX Quantum **2**, 030322 (2021).

[10] I. Cong, H. Levine, A. Keesling, D. Bluvstein, S. T. Wang, and M. D. Lukin, Phys. Rev. X **12**, 021049 (2022).

[11] X. Wu, X. Liang, Y. Tian, F. Yang, C. Chen, Y.-C. Liu, M. K. Tey, and L. You, Chinese Phys. B **30**, 020305 (2021).

[12] I. Bloch, J. Dalibard, and S. Nascimbène, Nat. Phys. **8**, 267 (2012).

[13] B. Opanchuk, R. Polkinghorne, O. Fialko, J. Brand, and P. D. Drummond, Ann. Phys. **525**, 866 (2013).

[14] J. Simon, W. S. Bakr, R. Ma, M. E. Tai, P. M. Preiss, and M. Greiner, Nature (London) **472**, 307 (2011).

[15] S. Kuhr, Natl. Sci. Rev. **3**, 170 (2016).

[16] E. T. Davletov, V. V. Tsyganok, V. A. Khlebnikov, D. A. Pershin, D. V. Shaykin, and A. V. Akimov, Phys. Rev. A **102**, 011302(R) (2020).

[17] V. A. Khlebnikov, D. A. Pershin, V. V. Tsyganok, E. T. Davletov, I. S. Cojocaru, E. S. Fedorova, A. A. Buchachenko, and A. V. Akimov, Phys. Rev. Lett. **123**, 213402 (2019).
[18] V. A. Khlebnikov, V. V. Tsyganok, D. A. Pershin, E. T. Davletov, E. Kuznetsova, and A. V. Akimov, Phys. Rev. A **103**, 023306 (2021).
[19] T. Maier, I. Ferrier-Barbut, H. Kadau, M. Schmitt, M. Wenzel, C. Wink, T. Pfau, K. Jachymski, and P. S. Julienne, Phys. Rev. A **92**, 060702(R) (2015).
[20] A. Frisch, M. Mark, K. Aikawa, F. Ferlaino, J. L. Bohn, C. Makrides, A. Petrov, and S. Kotochigova, Nature (London) **507**, 475 (2014).
[21] J. Stuhler, A. Griesmaier, T. Koch, M. Fattori, T. Pfau, S. Giovanazzi, P. Pedri, and L. Santos, Phys. Rev. Lett. **95**, 150406 (2005).
[22] A. J. Olson, D. L. Whitenack, and Y. P. Chen, Phys. Rev. A **88**, 043609 (2013).
[23] M. Lu, S. H. Youn, and B. L. Lev, Phys. Rev. Lett. **104**, 063001 (2010).
[24] A. Trautmann, P. Ilzhöfer, G. Durastante, C. Politi, M. Sohmen, M. J. Mark, and F. Ferlaino, Phys. Rev. Lett. **121**, 213601 (2018).
[25] E. Lucioni, L. Tanzi, A. Fregosi, J. Catani, S. Gozzini, M. Inguscio, A. Fioretti, C. Gabbanini, and G. Modugno, Phys. Rev. A **97**, 060701(R) (2018).
[26] M. Lu, N. Q. Burdick, S. H. Youn, and B. L. Lev, Phys. Rev. Lett. **107**, 190401 (2011).
[27] K. Aikawa, A. Frisch, M. Mark, S. Baier, A. Rietzler, R. Grimm, and F. Ferlaino, Phys. Rev. Lett. **108**, 210401 (2012).
[28] A. Frisch, M. Mark, K. Aikawa, S. Baier, R. Grimm, A. Petrov, S. Kotochigova, G. Quéméner, M. Lepers, O. Dulieu, and F. Ferlaino, Phys. Rev. Lett. **115**, 203201 (2015).
[29] L. Tanzi, E. Lucioni, F. Famà, J. Catani, A. Fioretti, C. Gabbanini, R. N. Bisset, L. Santos, and G. Modugno, Phys. Rev. Lett. **122**, 130405 (2019).
[30] L. W. Cheuk, M. A. Nichols, M. Okan, T. Gersdorf, V. V. Ramasesh, W. S. Bakr, T. Lompe, and M. W. Zwierlein, Phys. Rev. Lett. **114**, 193001 (2015).
[31] E. Haller, J. Hudson, A. Kelly, D. A. Cotta, B. Peaudecerf, G. D. Bruce, and S. Kuhr, Nat. Phys. **11**, 738 (2015).
[32] R. Yamamoto, J. Kobayashi, K. Kato, T. Kuno, Y. Sakura, and Y. Takahashi, Phys. Rev. A **96**, 033610 (2017).
[33] W. S. Bakr, J. I. Gillen, A. Peng, S. Fölling, and M. Greiner, Nature (London) **462**, 74 (2009).
[34] S. J. Thomson, L. S. Walker, T. L. Harte, and G. D. Bruce, Phys. Rev. A **94**, 051601(R) (2016).
[35] R. Yamamoto, J. Kobayashi, T. Kuno, K. Kato, and Y. Takahashi, New J. Phys. **18**, 023016 (2016).
[36] V. V. Tsyganok, D. A. Pershin, V. A. Khlebnikov, D. A. Kumpilov, I. A. Pyrkh, A. E. Rudnev, E. A. Fedotova, D. V. Gaifudinov, I. S. Cojocaru, K. A. Khoruzhii, P. A. Aksentsev, A. K. Zykova, and A. V. Akimov, Phys. Rev. A **107**, 023315 (2023).
[37] G. Ramola, R. Winkelmann, K. Chandrashekara, W. Alt, P. Xu, D. Meschede, and A. Alberti, Phys. Rev. Appl. **16**, 024041 (2021).
[38] A. Bertoldi, S. Bernon, T. Vanderbruggen, A. Landragin, and P. Bouyer, Opt. Lett. **35**, 3769 (2010).
[39] G. E. Marti, R. B. Hutson, A. Goban, S. L. Campbell, N. Poli, and J. Ye, Phys. Rev. Lett. **120**, 103201 (2018).
[40] P. L. Kapitza and P. A. M. Dirac, Math. Proc. Cambridge Philos. Soc. **29**, 297 (1933).
[41] S. Altshuler, L. M. Frantz, and R. Braunstein, Phys. Rev. Lett. **17**, 231 (1966).
[42] P. L. Gould, G. A. Ruff, and D. E. Pritchard, Phys. Rev. Lett. **56**, 827 (1986).
[43] B. Gadway, D. Pertot, R. Reimann, M. G. Cohen, and D. Schneble, Opt. Express **17**, 19173 (2009).
[44] D. A. Pershin, V. V. Tsyganok, V. V. Yaroshenko, V. A. Khlebnikov, E. T. Davletov, E. L. Svechnikov, V. N. Sorokin, P. V. Kapitanova, and A. V. Akimov, Bull. Lebedev Phys. Inst. **45**, 377 (2018).
[45] I. S. Cojocaru, S. V. Pyatchenkov, S. A. Snigirev, I. A. Luchnikov, E. S. Kalganova, G. A. Vishnyakova, D. N. Kublikova, V. S. Bushmakin, E. T. Davletov, V. V. Tsyganok, O. V. Belyaeva, A. Khoroshilov, V. N. Sorokin, D. D. Sukachev, and A. V. Akimov, Phys. Rev. A **95**, 012706 (2017).
[46] D. A. Pershin, V. V. Yaroshenko, V. V. Tsyganok, V. A. Khlebnikov, E. T. Davletov, D. V. Shaykin, E. R. Gadylshin, I. S. Cojocaru, E. L. Svechnikov, P. v. Kapitanova, and A. V. Akimov, Phys. Rev. A **102**, 043114 (2020).
[47] V. V. Tsyganok, D. A. Pershin, E. T. Davletov, V. A. Khlebnikov, and A. V. Akimov, Phys. Rev. A **100**, 042502 (2019).
[48] V. V. Tsyganok, V. A. Khlebnikov, E. S. Kalganova, D. A. Pershin, E. T. Davletov, I. S. Cojocaru, I. A. Luchnikov, A. V. Berezutskii, V. S. Bushmakin, V. N. Sorokin, and A. V. Akimov, J. Phys. B: At. Mol. Opt. Phys. **51**, 165001 (2018).
[49] T. A. Savard, K. M. O'Hara, and J. E. Thomas, Phys. Rev. A **56**, R1095(R) (1997).
[50] D. Sukachev, S. Fedorov, I. Tolstikhina, D. Tregubov, E. Kalganova, G. Vishnyakova, A. Golovizin, N. Kolachevsky, K. Khabarova, and V. Sorokin, Phys. Rev. A **94**, 022512 (2016).